Journal of Nuclear Materials 393 (2009) 321–327

Contents lists available at ScienceDirect

Journal of Nuclear Materials

journal homepage: www.elsevier.com/locate/jnucmat

First-principles study on cerium ion behavior in irradiated cerium dioxide

Misako Iwasawa [a,*], Toshiharu Ohnuma [a], Ying Chen [b], Yasunori Kaneta [b], Hua-Yun Geng [b], Akihiro Iwase [c], Motoyasu Kinoshita [b,d,e]

[a] Materials Science Research Laboratory, Central Research Institute of Electric Power Industry, 2-11-1 Iwado-kita, Komae-shi, Tokyo 201-8511, Japan
[b] Department of Systems Innovation, The University of Tokyo, 7-3-1 Hongo, Bunkyo-ku, Tokyo 113-8656, Japan
[c] Department of Materials Science, Osaka Prefecture University, Gakuen-cho, Naka-ku, Sakai-shi, Osaka 599-8531, Japan
[d] Nuclear Technology Research Laboratory, Central Research Institute of Electric Power Industry, 2-11-1 Iwado-kita, Komae-shi, Tokyo 201-8511, Japan
[e] Japan Atomic Energy Agency, Tokai-mura, Naka-gun, Ibaraki 319-1195, Japan

ARTICLE INFO

Article history:
Received 23 January 2009
Accepted 17 June 2009

ABSTRACT

In order to clarify, from the electronic structure, the origin of the appearance of the tri-valent Ce state in irradiated cerium dioxide with swift heavy ions, we performed comprehensive first-principles calculations on various defective structures in cerium dioxide. The calculated results show that an oxygen mono-vacancy or an oxygen Frenkel pair can induce two tri-valent Ce states neighboring the oxygen vacancy. The calculation of the oxygen Frenkel pair further reveals that an interstitial oxygen atom that moves from the lattice position and an oxygen atom on the lattice can form a dimer that behaves as an oxygen molecule of negative di-valence. This bonding state can also produce excess electrons and the tri-valent Ce state in cerium dioxide.

1. Introduction

Recently, irradiation effects on cerium dioxide (CeO_2) have been studied extensively as a simulation material of uranium dioxide (UO_2) [1–4]. Under high burn-up conditions in nuclear reactors, UO_2 shows various structural evolutions that result in some complicated subgrain structures. One of them is known as the rim structure [5]. Because of various difficulties in handling UO_2 directly in experiments, CeO_2 has been used instead of UO_2 to study the material properties of UO_2 with respect to structural changes in irradiation, electron beam or heavy ion irradiation experiments, because they have the same fluorite (CaF_2)-type crystal structure and are similar oxide materials.

CeO_2 is known to be a typical insulator. In the ordinary ground state of CeO_2, the Ce ion is in the tetra-valent (Ce^{4+}) state without 4f electrons. However, Ohno et al. observed a tri-valent (Ce^{3+}) state spectrum in bulk CeO_2 under the irradiation with swift heavy ions [6]. They reported that an increase in the intensity of the X-ray photoelectron spectroscopy (XPS) spectrum corresponds to the Ce^{3+} state with increasing Xe irradiation fluence. They also observed the decrease of the first coordination number from 8 to 7 or 6 around the Ce ion by analyzing the extended X-ray absorption fine structure (EXAFS) spectrum. One may attribute these phenomena to surface effects and/or a kind of deoxidation (reduction) from CeO_2 to the sesquioxide Ce_2O_3. However, consistency among the experimental results of X-ray diffraction, EXAFS and electric conductivity measurements [7] for irradiated CeO_2 supports the existence of the Ce^{3+} state in bulk CeO_2, where irradiation damage occurs from the surface to a depth of several hundred nanometers.

One possible origin of the Ce^{3+} state is considered to be the excess electrons generated from oxygen vacancies by the irradiation. However, the generation of oxygen vacancies requires a change of the composition, that is, a reduction of CeO_2. On the other hand, Yasunaga et al. observed defect clusters of interstitial type dislocation loops lying on the {1 1 1} plane in CeO_2 irradiated with an electron beam with the energy range of 200–1000 keV [3]. On the basis of the results of the experiment, they proposed that the dislocation loops consist of interstitial oxygen clusters. This experimental result suggests that the oxygen atoms that are distorted or that migrate by irradiation can stay in bulk, forming interstitial-vacancy (Frenkel) pairs that become the initial cores of the interstitial clusters. Moreover, the possibility arises that the Frenkel pair may generate a Ce^{3+} ion, by which the composition remains invariant. One focus of the present study is to calculate the electronic structures of CeO_2 in various defect models to confirm the effect of the oxygen vacancy and the oxygen Frenkel pair on the generation of Ce^{3+}.

There are some difficulties in the first-principles study of Ce^{3+}. In Ce_2O_3, the Ce^{3+} ion in the $4f^1$ state is stable and shows an energy gap at the Fermi level in XPS and bremsstrahlung isochromat spectroscopy experiments [8]. However, these futures are not obvious in theoretical first-principles calculations. For example, calculations based on the local density approximation (LDA) or the generalized gradient approximation (GGA) reveal metallic states for Ce_2O_3 and for CeO_2 with oxygen vacancies. In earlier calculations,

* Corresponding author.
E-mail address: misa0130@gamma.ocn.ne.jp (M. Iwasawa).

0022-3115/$ - see front matter © 2009 Elsevier B.V. All rights reserved.
doi:10.1016/j.jnucmat.2009.06.026

the valence band model (conventional LDA calculation) was adopted to describe the Ce^{4+} electronic state of CeO_2 and the core state model (the $4f^1$ state is treated as the core state) was used to describe the Ce^{3+} electronic state of Ce_2O_3; then, both materials could be described as insulators [9,10]. Such a case-by-case treatment is adequate for systems in which the valence state of all Ce ions is the same, such as in perfect CeO_2 or Ce_2O_3. However, it is not suited for the mixed valence systems of defective CeO_2. Recent calculations have shown that adopting additional intra-atomic (on site) Coulomb interactions, such as the LDA + U or GGA + U method [11–13], for 4f electrons on Ce is effective for describing the insulating nature of Ce_2O_3 and CeO_2 with oxygen vacancies [14–19]. Fabris et al. showed that multiple valence in defective CeO_2 is reproduced by the LDA/GGA + U method with the Hubbard effective Coulomb repulsion parameters $U = 3.0$ eV for LDA and $U = 1.5$ eV for GGA [14]. Castleton et al. [17], Andersson et al. [18], and Loschen et al. [19] also studied defective CeO_2 to obtain an appropriate U value in relation to the experimentally identified physical properties. The range of the U value was selected to be from about 3–7 eV in the LDA calculations, and from about 1.5–5.5 eV in the GGA calculations.

For the electronic structure of UO_2, we previously calculated the lattice deformation and defect formation energies of various defect structures, using the GGA+U [20] and the LDA+U method [21]. Zero or negative formation energy for a single oxygen interstitial had been calculated, and found to be consistent with the well known fact that UO_2 can be oxidized more easily, and becomes U_4O_9.

Our main aim of the present study is to clarify the origin of the Ce^{3+} state spectrum observed in Ohno et al.'s experiment. We perform comprehensive first-principles calculations for CeO_2, introducing various defects, in a similar way as in our previous work on defective UO_2 [20]. We then discuss the relationship between defects types and the appearance of the Ce^{3+} ion by comparing our calculations with available experimental results for irradiated CeO_2.

In the next section, we describe the calculation method and defective structure models employed. In Section 3, the calculated results and discussion on the electronic structure, lattice deformation and defect formation energies are presented. Finally, we summarize our results in Section 4.

2. Calculation method and calculation models

All calculations in the present work were carried out by the projector augmented-wave method [22,23], as implemented in the Vienna ab initio Simulation Package (VASP) [24]. Spin polarization was taken into account in our calculations, except for the calculation for perfect CeO_2 (no defects). In this work, we employed the GGA + U method, and the Hubbard U correction was introduced to the 4f orbital of all Ce atoms in the cell using the method proposed by Dudarev et al. [13]. The values we adopted were $U = 5.5$ eV and $J = 0.0$ eV, proposed by Castleton et al. [17], because these values were evaluated for the CeO_2 system with oxygen vacancies. The Perdew–Burke–Ernzerhof (PBE)–GGA [25] was used for the exchange correlation term, as in our previous work on UO_2 [20]. The cut-off energy of 500.0 eV for the plane wave expansion and a $3 \times 3 \times 3$ k-mesh described by Monkhorst–Pack [26] are applied for all calculation models. All structural parameters, including lattice constants, cell shapes and all atom positions, were relaxed using the RMM-DIIS algorithm [27]. The convergence of our self-consistent calculations was estimated to be less than 10^{-4} eV for the total energy.

A supercell of 96 atoms, $Ce_{32}O_{64}$ ($2 \times 2 \times 2$ unit cells of Ce_4O_8 CaF_2 structure), was used in this study as a basic model for defective CeO_2 and expressions. The periodic boundary condition was adopted. Nine defect models are introduced in the present study: (1) oxygen mono-vacancy (O_V) model, which is formed by removing one oxygen atom from the supercell, $Ce_{32}O_{63}$; (2) oxygen Frenkel pair (O_{FP}) model, in which one oxygen atom on a sublattice site is moved to the farthest interstitial position, $Ce_{32}O_{64}$; (3) oxygen interstitial (O_I) model, which is formed by adding one oxygen atom to an interstitial position, $Ce_{32}O_{65}$; (4) Ce mono-vacancy (Ce_V) model, which is formed by the removal of one Ce atom from the supercell, $Ce_{31}O_{64}$; (5) Ce interstitial (Ce_I) model, which is formed by placing one Ce atom into an interstitial position, $Ce_{33}O_{64}$; (6) Ce–O di-vacancy ($(CeO)_V$) model, in which one Ce atom and the nearest oxygen atom are removed from the supercell, $Ce_{31}O_{63}$; (7) CeO_2 tri-vacancy ($(CeO_2)_V$) model in the form of a Shottky trio formed by removing one Ce atom and two neighboring oxygen atoms from the supercell, $Ce_{31}O_{62}$; (8) antisite Ce on oxygen site (Ce_O) model, $Ce_{33}O_{63}$ and (9) antisite oxygen atom on Ce site (O_{Ce}) model, $Ce_{31}O_{65}$.

In the O_I and O_{FP} models, we tested two kinds of initial defect configurations: one where an interstitial oxygen atom is placed just at the center of the oxygen cube formed from eight oxygen atoms on a cubic sublattice (called "center type" hereafter), the other is an interstitial oxygen atom inserted near a sublattice oxygen atom (called "lattice type"). According to the vacancy configurations, we tested three types of the $(CeO_2)_V$ models: (7-a) the two nearest oxygen atoms were removed; (7-b) two of the second nearest oxygen atoms were removed; (7-c) the two removed oxygen atoms and one Ce atom are positioned on a line along the [1 1 1] direction.

The defect formation energy is defined as:

$$E^F_{DX} = E_D(X) - E^N \pm E_X,$$

where E^F_{DX} is the defect formation energy on atom X (X = Ce, O), $E_D(X)$ is the calculated internal energy of the cell with defect X, E^N is the internal energy of the perfect crystal without defects, and E_X is the internal energy of a pure substance formed of X-atoms in a reference state. The positive and negative signs before E_X correspond to an X vacancy and an X interstitial atom, respectively. Ce metal in the fcc phase (lattice constant is calculated as 4.83 Å after relaxation), and the O_2 molecule (O–O distance is calculated as 1.23 Å) in a cubic cell with a fixed edge of 10 Å are taken as the reference states of Ce and oxygen, respectively. For fcc–Ce, the internal energy was also calculated by the PBE-GGA+U method using the same Hubbard U value, $U = 5.5$ eV.

It should be noted that the defect formation energies calculated by the above procedure might disagree with experimental values. As tested by Fabris et al. [14] and Andersson et al. [18], the calculated value of the defect formation energy depends largely on the choice of LDA or GGA, and on the value of the Hubbard U. In addition, neglecting the spin–orbit interactions in present calculations induces further error. Since the spin–orbit splitting of the $4f^1$ state on the Ce atom is estimated to be about 0.3 eV, we predict that the error in our calculated values of total energy will be on the order of 0.5 eV, therefore, it is necessary to take care when comparing the stability among the defect systems used in this work.

3. Results and discussion

3.1. Oxygen mono-vacancy model

Although the O_V model has already been studied so far in the references [14–19], our results provide more information on the dependence of the electronic structure properties on the defect type, obtained through our series calculations carried out within the same theoretical framework and using a consistent parameter set.

We found that when the initial configuration of atoms in the supercell has lower point symmetry than cubic symmetry at the vacancy site, two excess electrons from the oxygen vacancy are transferred to two of four nearest-neighbor Ce atoms of the oxygen vacancy [28]. This result is almost the same as that described by Castleton et al. [17].

Fig. 1 shows the calculated relaxed defective structure (Fig. 1a) and the schematic figure of the oxygen cubic sublattice around the oxygen vacancy site (Fig. 1b), where distortions of atomic positions are emphasized. All four nearest-neighbor Ce atoms of the vacancy site move outward from their original positions, because attractive interactions between the Ce atoms and the oxygen atom which was at the vacancy site have been removed. The distance between Ce(1) or Ce(2) and the oxygen vacancy site are estimated to be 2.52 Å, and those of Ce(3) or Ce(4) to be 2.57 Å, they are larger than the Ce–O distance of 2.38 Å in perfect CeO_2. The outward shifts in the positions of Ce(1) and Ce(2) are smaller than those of Ce(3) and Ce(4). These two types of atomic distances for the four nearest-neighbor Ce atoms are caused by different charge states between Ce(1) or Ce(2) and Ce(3) or Ce(4). The charge state of the Ce(1) or Ce(2) atom is almost Ce^{3+} state and that of the Ce(3) or Ce(4) is Ce^{4+} state, which we will discuss afterwards. The oxygen atoms around the vacancy site shift inward from the original positions, because repulsive interactions between the oxygen atom which was at the vacancy site and the surrounding oxygen atoms have been removed. We can see that the shift of one oxygen atom is larger than those of the others, as depicted in Fig. 1b. This selective inward shift is also caused by the different charge states in the Ce atoms around the vacancy site. The inward shifts of the oxygen around Ce^{3+} ions are inhibited by the extra electrons than those around Ce^{4+} ions, then the inward shift of the oxygen whose original location is furthest from Ce^{3+} ions results in the largest. As a result of the relocalization of atoms, the lattice constants are slightly larger than those of perfect CeO_2, as shown in Table 1. Table 1 also shows the calculated lattice constants of perfect CeO_2 as well as other defect models in this work.

Fig. 2 shows total density of states (TDOS) and site-projected density of states (PDOS), such as d- and f-components on Ce atoms (in green and blue), p-component on oxygen atoms (in red) and f-components of Ce(1) and Ce(2) atoms (in light blue). The upper and lower parts indicate majority spin and minority spin components, respectively. One can see that the valence bands mainly consist of oxygen p-components (2p bands), whereas bands mainly from d-components of Ce (5d bands) are located at about 11.0 eV. It is worth noting that at 6.5 eV, there is a sharp peak (in light blue) that consists of two degenerated bands of f-components originating almost exclusively from Ce(1) and Ce(2) atoms. The difference in allocated electrons between majority and minority spins is 0.96, whereas for other Ce atoms, the f-components are nearly zero, which implies that Ce(1) and Ce(2) atoms have each gained one extra electron compared with other Ce atoms, resulting in the valence changing from Ce^{4+} to Ce^{3+} at Ce(1) and Ce(2). These $4f^1$ states at Ce^{3+} ions might have two magnetic configurations, ferromagnetic and antiferromagnetic. In this paper, we show mainly the ferromagnetic one [29]. The Fermi level is located at 7.0 eV in Fig. 2. There is a large peak at 7.5 eV in Fig. 2; it is composed of the f-components of Ce(3), Ce(4) and other Ce atoms. Because these Ce atoms have almost no occupied f-components, their f bands undergo less splitting due to the Hubbard U term. On the other hand, the peak at about 12.0 eV results from the splitting of the state at around 7.0 eV by 5.0 eV; this is the right $+U$ effect.

Fig. 3 shows the partial charge density corresponding to the sharp peak at 6.5 eV shown in Fig. 2. The density was projected onto the $(-1\,1\,1)$ plane, which contains the Ce(1), Ce(2) and Ce(4) atoms. The localized states of extra $4f^1$ electrons on Ce(1) and Ce(2) can be seen clearly. These extra electrons originating from the removal of the oxygen atom induces the valence change of Ce atoms.

3.2. Oxygen Frenkel pair model

In the O_{FP} model with one oxygen Frenkel pair in the supercell, we found at least two stable interstitial sites according to the initial positions of the oxygen atoms: one is at the center (center type) and the other is off-center (lattice type). Fig. 4a shows the relaxed cell lattice of the center type and Fig. 4b shows that of the lattice type. The TDOS and PDOS of these defective structures are shown in Figs. 5a and b, respectively.

In the case of the center type (Fig. 5a), the top of the valence band at about 6.0 eV is composed mainly of p-components of the oxygen atom at the interstitial site. In Fig. 5a, all of six p bands of the interstitial oxygen are fully occupied, which means no excess electrons can be transmitted to Ce atoms. Therefore, the occupation number of f-components is nearly zero and f bands do not split but show a large peak at around 8.0 eV, above the Fermi level (6.7 eV). The calculated magnetic moment is almost 0.0 μ_B.

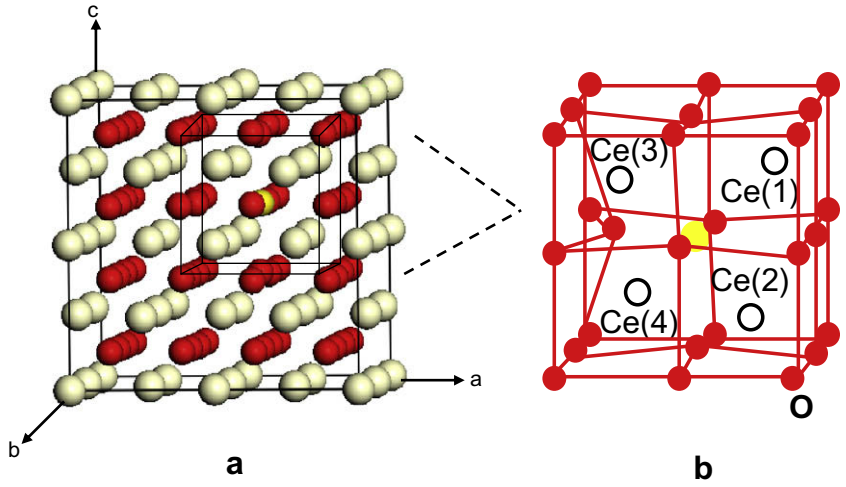

Fig. 1. Relaxed cell structure of the O_V model: (a) full supercell of $Ce_{32}O_{63}$ and (b) around the oxygen vacancy site. In (b), displacement of atoms is emphasized. Here and in the following figures, white circles are Ce atoms, red circles are oxygen atoms, and yellow circles indicate vacancy sites. The same direction of axes *a*, *b* and *c* are also used in the following figures. (For interpretation of the references to colour in this figure legend, the reader is referred to the web version of this article.)

Table 1
Calculated lattice parameters, defect formation volumes and defect formation energies of relaxed structures of defective systems.

Defective system[a]	Lattice constants (Å)			Equilibrium volume (Å^3)	Defect formation volume (Å^3)[b]	Defect formation energy (eV)
	a	b	c			
O_V	11.01	11.01	11.01	1334.33	10.15	2.7
O_{FP} (center type)	11.00	11.00	11.00	1330.45	6.27	3.9
O_{FP} (lattice type)	11.04	11.04	11.03	1345.47	21.29	4.6
O_I (center type)	10.99	10.99	10.99	1328.10	3.92	3.0
O_I (lattice type)	11.02	11.02	11.01	1336.82	12.64	2.1
Ce_I	11.09	11.08	11.08	1360.24	36.06	−0.2
Ce_O	11.09	11.10	11.09	1364.42	40.24	3.4
$(CeO)_V$	10.99	10.99	10.99	1328.40	4.22	15.5
$(CeO_2)_V$ (a)	10.99	11.02	10.99	1329.37	5.19	14.7
$(CeO_2)_V$ (b)	11.00	11.00	10.99	1329.57	5.39	14.1
$(CeO_2)_V$ (c)	10.99	10.99	10.99	1327.18	3.00	14.3
Ce_V	10.99	10.99	10.99	1327.95	3.77	16.8
O_{Ce}	10.98	10.98	10.98	1324.15	−0.03	19.6
Perfect	10.98	10.98	10.98	1324.18	–	–

[a] All models and types are described in the text.
[b] Perfect volume is taken in the standard.

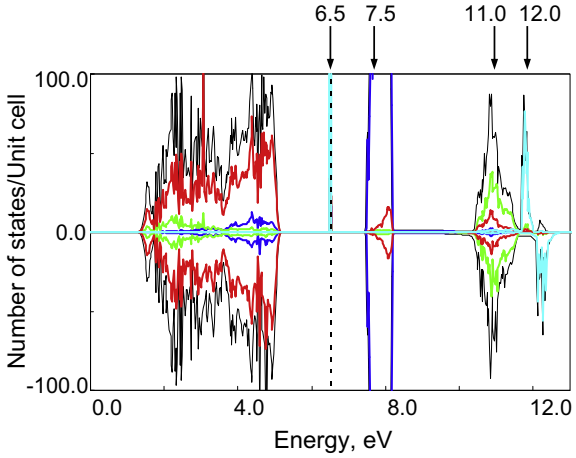

Fig. 2. Total DOS (thin line) and PDOS of the O_V model. Here and in the following figures, red line indicates p-components of oxygen, green line indicates d-components of Ce, blue line indicates f-components of Ce atoms, and the vertical dotted line indicates the top of the valence band. Light blue line indicates f-components of Ce(1) and Ce(2) depicted in Fig. 1b. (For interpretation of the references to colour in this figure legend, the reader is referred to the web version of this article.)

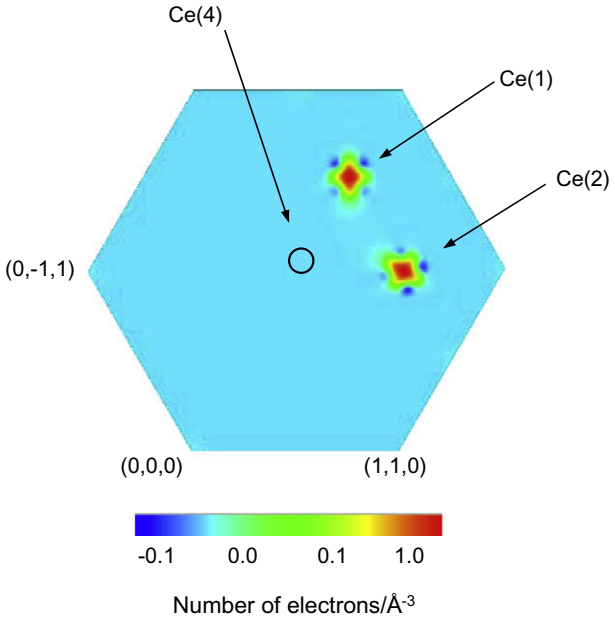

Fig. 3. Partial charge density distributions of the O_V model. The charges corresponding to the sharp peak near the top of the valence band (at E = 6.5 eV in Fig. 2) are projected onto the (−1 1 1) plane including the Ce(1) and Ce(2) atoms.

In the case of the lattice type, however, two split peaks at 6.4 and 11.7 eV, which consisted mainly of the f-components on the two Ce atoms near the vacancy site, are observed, as shown in Fig. 5b. This situation is very similar to that of the O_V model (Fig. 2), in which there are excess electrons that result in the two Ce^{3+} ions. Fig. 6a shows the partial charge distribution corresponding to the sharp peak at 6.4 eV in Fig. 5b projected onto the (1 −1 0) plane. It can be seen that the lattice-type O_{FP} model can also generate the Ce^{3+} ions. Moreover, a very sharp peak appears on the deep energy side, at about 0.5 eV, in Fig. 5b, it consists of p-components from the oxygen atoms near the interstitial site. Fig. 6b shows the projection of the partial charge distributions corresponding to this peak onto the (0 0 1) plane where two oxygen atoms are included: one originates from the interstitial oxygen after being removed from a lattice site to form an oxygen vacancy; the other is the one at the oxygen sublattice site. Fig. 6b shows clearly that the two oxygen atoms form a bonding state showing a dimer or dumbbell structure; its bond length is calculated to be 1.44 Å. This lattice-type O_{FP} model gives a calculated total magnetic moment of 1.8 μ_B.

The distribution of distances between neighboring atoms is calculated and compared with the EXAFS experimental data shown in the Fig. 2 in Ref. [6], although these experimental data contain some error in the absolute value of distances. The O–O neighbors could not be observed because the Ce K-edge was used in the EXAFS experiment. Here we plot Ce–Ce and Ce–O distances in Fig. 7. It can be seen that the Ce–O distance was distributed in the range from 2.29 to 2.60 Å, and the Ce–Ce distance was distributed from 3.78 to 4.19 Å in the two groups. Obviously, these characteristics correspond to the main feature of the peak intensity and the broadening in the EXAFS spectrum.

The calculation above indicates that the Ce^{3+} ion can originate from the oxygen Frenkel pair when the configuration of defects is well considered. This conclusion is based on not the usual stoichiometric consideration but the discussion on the electronic structures obtained by the first principles calculations. Moreover,

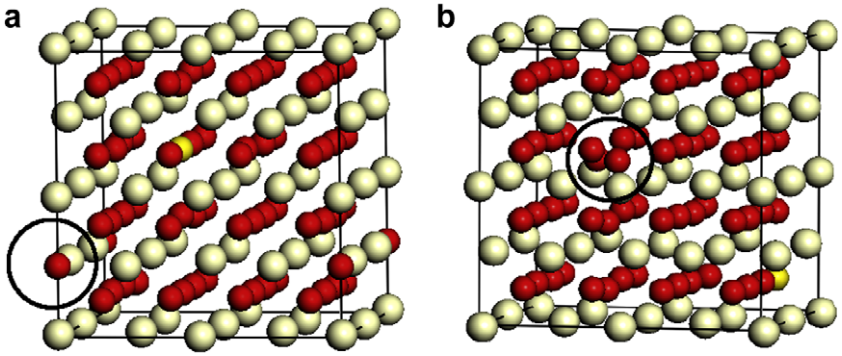

Fig. 4. Relaxed cell structure of the O_{FP} model: (a) the center type and (b) the lattice type. Black circular outline indicates each interstitial site.

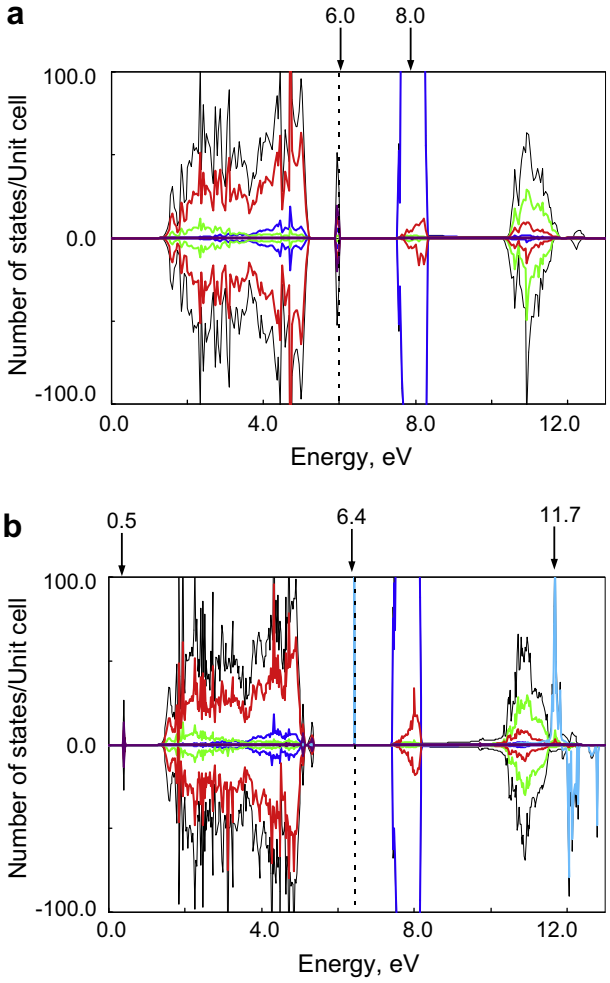

Fig. 5. TDOS (thin line) and PDOS of the O_{FP} model: (a) the center type and (b) the lattice type. Purple line indicates the p-components of the interstitial oxygen atom. Light blue line indicates f-components of Ce^{3+} ions, which are described in the text in detail. (For interpretation of the references to colour in this figure legend, the reader is referred to the web version of this article.)

this consideration agrees qualitatively with the experimental results of EXAFS and XPS.

3.3. Oxygen interstitial model

It is well known that the simple defective structures generated by irradiation are oxygen vacancies, oxygen Frenkel pairs and Ce Frenkel pairs. It is difficult for other defect systems, such as oxygen interstitials or Ce vacancies, to exist in the usual irradiation environment. However, in a restricted local region, there is some possibility for these defective systems to exist, so we comprehensively calculate all mono-defective systems of CeO_2, though these are not more realistic than O_V or O_{FP}. In the O_I model with one additional oxygen atom at around the interstitial site in the supercell, similar to the description in the previous subsection, the interstitial oxygen atom can have at least two stable positions around the interstitial site: the center type and the lattice type.

Fig. 8a and b show the calculated relaxed cell structures of the center type and the lattice type, respectively. In Fig. 8b, it is found that a bond between two oxygen atoms exists at the distance of 1.44 Å, which is longer than that of the O_2 molecule (1.23 Å in the present calculation). This dimer is on a plane parallel to the (0 0 1) plane, similar to the O_{FP} model, so the lattice constants of *a*- and *b*-axes are slightly longer than that of the *c*-axis, as shown in Table 1.

Fig. 9a shows the TDOS and PDOS of the center-type O_I. In the majority spin of DOS in Fig. 9a, two peaks at about 1.2 and 5.0 eV (purple lines) consist of p-components of the interstitial oxygen atom. In the minority spin part, two peaks, which also consist of p-components of the interstitial oxygen atom, are observed at about 5.5 eV, and the Fermi level is located in the pseudogap between these peaks. The partial occupation of the p band causes a total magnetic moment of 1.8 μ_B.

Fig. 9b shows the TDOS and PDOS of the lattice-type O_I. The total magnetic moment is calculated to be 0.0 μ_B. The interstitial oxygen atom of the lattice-type O_I model could form a dimer with an oxygen atom on the lattice, as shown in Fig. 8b. It shows that the p-components of this oxygen dimer, indicated in purple, exhibit a large splitting wherein the six p orbital states of two oxygen atoms split into five peaks. The states at around −0.6 and 0.6 eV are bonding states of dimer forming oxygens, those at 5.2 and 5.6 eV are mainly nonbonding states, and that at 9.9 eV is the antibonding state. The first two energy levels are occupied by six electrons. The third and fourth levels are occupied by two electrons of the original oxygen atoms and two electrons from Ce^{4+}, so the oxygen dimer becomes O_2^{2-}. This gives the following picture of the interstitial oxygen cluster in irradiated CeO_2: the additional interstitial oxygen atom is bonded to a lattice oxygen atom and this oxygen dimer behaves like a pseudo lattice oxygen atom.

3.4. Other defect models

Our calculation based on the GGA + *U* method leads to the rational explanation that the excess electrons from an additional Ce or from a vacancy due to the removal of oxygen atoms generate the Ce^{3+} ions. The Ce_I model and the Ce_O model showed four and

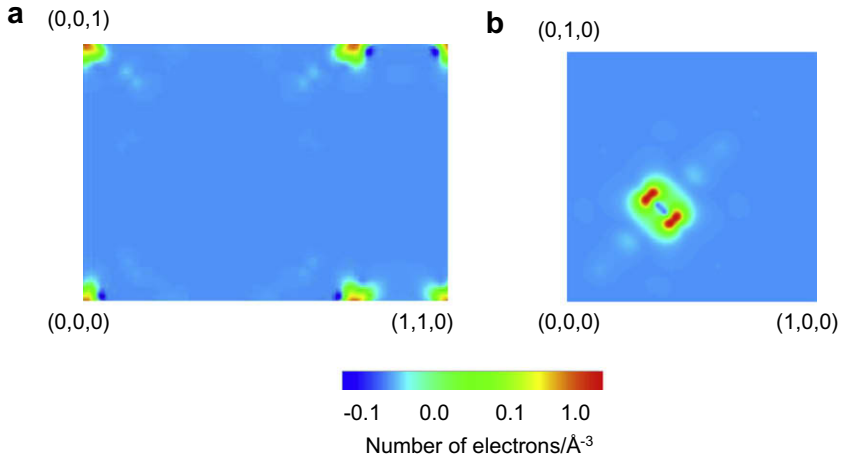

Fig. 6. Partial charge density distributions of the lattice type O_{FP} model. The charges corresponding to (a) the sharp peak near the top of the valence band (at $E = 6.4$ eV in Fig. 5(b)) are projected onto the (1 −1 0) plane including the Ce^{3+} ions and (b) the peaks at $E = 0.5$ eV in Fig. 5(b) are projected onto the (0 0 1) plane.

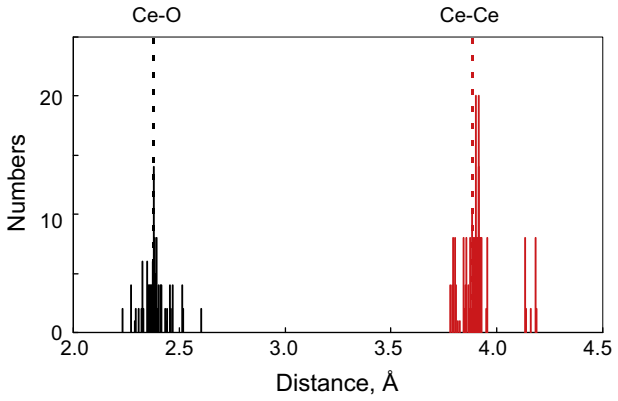

Fig. 7. The distance distribution of the lattice type O_{FP} model. Black lines indicate the Ce–O distances and red lines indicate the Ce–Ce distances. Dotted black and red lines indicate the Ce–O and Ce–Ce distances of the perfect CeO_2, respectively. (For interpretation of the references to colour in this figure legend, the reader is referred to the web version of this article.)

six Ce^{3+} ions, respectively, and there is a tendency for Ce^{3+} ions to gather as nearest-neighbors (or clustering) on lattice points around a given defect point. It can be seen that the vacancy formation volumes of these defect types are larger than those of other oxygen defect systems shown in Table 1.

The O_{Ce} model, the Ce_V model and $(CeO)_V$ model have excess oxygen atoms. Their electronic structures are similar to that of the O_I model. The three types of the $(CeO_2)_V$ model have neutral compositions of Ce and oxygen, and their electronic structures do not show Ce^{3+} ions.

3.5. Defect formation energy

The estimated defect formation energies are listed in Table 1, as well as the formation volumes. It can be seen that almost all defective structures have positive formation energies, except the Ce_I model. It can be seen that the reduction of CeO_2 to Ce_2O_3 with Ce_I accompanies a large lattice volume expansion. It is also noted that the defect formation energies in models where Ce^{3+} ions appear are all around 3.0 eV, whereas the values of other models are all larger than 14.0 eV.

Although it is well known that the accuracy of the calculated total energy values are affected by the approximations employed and the parameters used, our calculations of formation energies within the same theoretical framework using consistent parameters provide relative trends of the formation of various types of defects. The lattice-type O_{FP} model has a high possibility of existing, as well as the O_V model. The lattice-type O_I model has lower energy than the center type, however, the lattice-type O_{FP} model has higher formation energy than the center type. The reason for this must be investigated further.

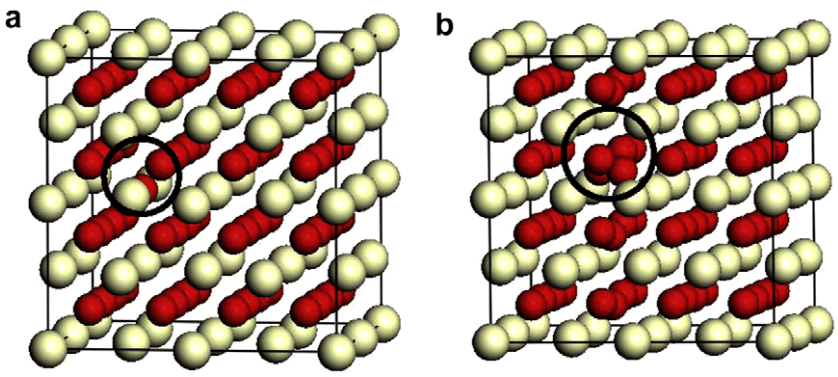

Fig. 8. Relaxed cell structure of the O_I model: (a) the center type and (b) the lattice type. Black circular outline indicates the each interstitial site.

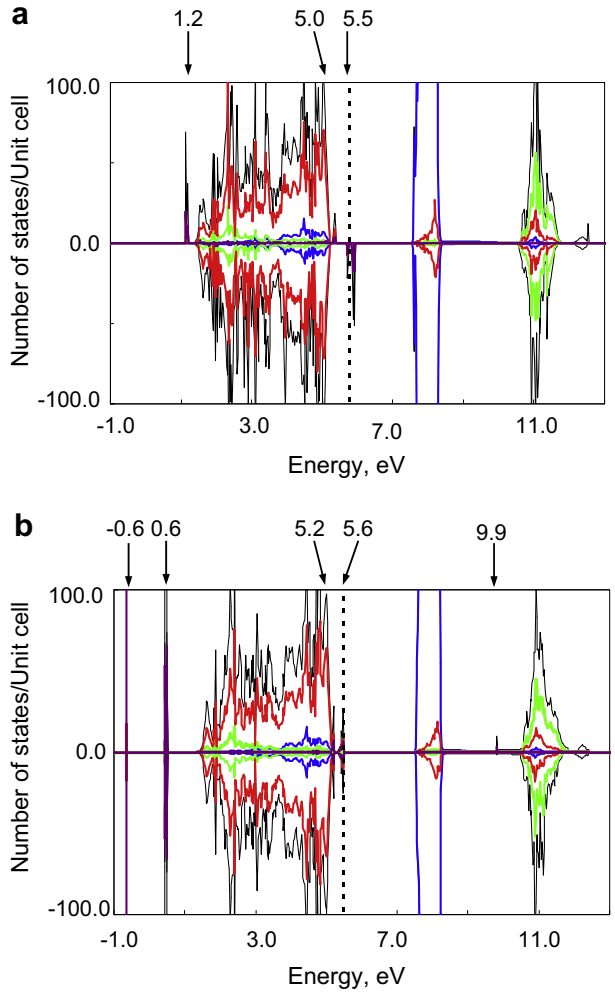

Fig. 9. TDOS (thin line) and PDOS of the O_I model: (a) the center type and (b) the lattice type. Purple line indicates p-components of the interstitial oxygen atom. (For interpretation of the references to colour in this figure legend, the reader is referred to the web version of this article.)

4. Conclusion

We performed first-principles calculations to clarify the origin of the Ce^{3+} state spectrum observed by XPS of irradiated CeO_2. By the GGA + U method, we calculated the electronic structures of defective CeO_2, with introducing various point defects systematically. We showed that the Ce^{3+} ion in CeO_2 originates not only from the oxygen vacancy but also from the oxygen Frenkel pair. This means that deoxidation (reduction) is not the only means of producing Ce^{3+} ions in CeO_2, but that displacement of oxygen from the sublattice position to the interstitial region can also produce Ce^{3+} ions. The interstitial oxygen atom can have metastable positions at the interstitial site as local minimum of energy. Among the two oxygen atoms that form the O_2^{2-} dimer, the bonding state of the interstitial atom and a lattice oxygen atom can provide two excess electrons to Ce^{4+} ions. This explains the EXAFS and XPS experimental observations on irradiated CeO_2.

Acknowledgement

This study was financially supported by the Budget for Nuclear Research of the Ministry of Education, Culture, Sports, Science and Technology, based on the screening and counseling by the Atomic Energy Commission.

References

[1] K. Yasunaga, K. Yasuda, S. Matsumura, T. Sonoda, Nucl. Instr. and Meth. Phys. Res. B 250 (2006) 114.
[2] T. Sonoda, M. Kinoshita, Y. Chimi, N. Ishikawa, M. Sataka, A. Iwase, Nucl. Instr. and Meth. Phys. Res. B 250 (2006) 254.
[3] K. Yasunaga, K. Yasuda, S. Matsumura, T. Sonoda, Nucl. Instr. and Meth. Phys. Res. B 266 (2008) 2877.
[4] T. Sonoda, M. Kinoshita, N. Ishikawa, M. Sataka, Y. Chimi, N. Okubo, A. Iwase, K. Yasunaga, Nucl. Instr. and Meth. Phys. Res. B 266 (2008) 2882.
[5] T. Sonoda, M. Kinoshita, I.L.F. Ray, T. Wiss, H. Thiele, D. Pellottiero, V.V. Rondinella, Hj. Matzke, Nucl. Instr. and Meth. Phys. Res. B 191 (2002) 622.
[6] H. Ohno, A. Iwase, D. Matsumura, Y. Nishihata, J. Mizuki, N. Ishikawa, Y. Baba, N. Hirao, T. Sonoda, M. Kinoshita, Nucl. Instr. and Meth. Phys. Res. B 266 (2008) 3013.
[7] A. Iwase, H. Ohno, submitted for publication.
[8] J.W. Allen, J. Magn. Magn. Mater. 47–48 (1985) 168.
[9] N.V. Skorodumova, R. Ahuja, S.I. Simak, I.A. Abrikosov, B. Johansson, B.I. Lundqvist, Phys. Rev. B 64 (2001) 115108.
[10] N.V. Skorodumova, S.I. Simak, B.I. Lundqvist, I.A. Abrikosov, B. Johansson, Phys. Rev. Lett. 89 (16) (2002) 166601.
[11] V.I. Anisimov, J. Zaanen, O.K. Andersen, Phys. Rev. B 44 (1991) 943.
[12] V.I. Anisimov, I.V. Solovyev, M.A. Korotin, M.T. Czyzyk, G.A. Sawatzky, Phys. Rev. B 48 (1993) 16929.
[13] S.L. Dudarev, G.A. Botton, S.Y. Savrasov, C.J. Humphreys, A.P. Sutton, Phys. Rev. B 57 (1998) 1505.
[14] S. Fabris, S. de Gironcoli, S. Baroni, G. Vicario, G. Balducci, Phys. Rev. B 71 (2005) 041102 (R).
[15] G. Kresse, P. Blaha, J.L.F. Da Silva, M.V. Ganduglia-Pirovano, Phys. Rev. B 72 (2005) 237101.
[16] S. Fabris, S. de Gironcoli, S. Baroni, G. Vicario, G. Balducci, Phys. Rev. B 72 (2005) 237102.
[17] C.W.M. Castleton, J. Kullgren, K. Hermansson, J. Chem. Phys. 127 (2007) 244704.
[18] D.A. Andersson, S.I. Simak, B. Johansson, I.A. Abrikosov, N.V. Skorodumova, Phys. Rev. B 75 (2007) 035109.
[19] C. Loschen, J. Carrasco, K.M. Neyman, F. Illas, Phys. Rev. B 75 (2007) 035115.
[20] M. Iwasawa, Y. Chen, Y. Kaneta, T. Ohnuma, H.Y. Geng, M. Kinoshita, Mater. Trans. 47 (2006) 2651.
[21] H.Y. Geng, Y. Chen, Y. Kaneta, M. Iwasawa, T. Ohnuma, M. Kinoshita, Phys. Rev. B 77 (2008) 104120.
[22] P.E. Blochl, Phys. Rev. B 50 (1994) 17953.
[23] G. Kresse, D. Joubert, Phys. Rev. B 59 (1999) 1758.
[24] G. Kresse, J. Furthmüller, Phys. Rev. B 54 (1996) 11169.
[25] J.P. Perdew, K. Burke, M. Ernzerhof, Phys. Rev. Lett. 77 (1996) 3865.
[26] H.J. Monkhorst, J.D. Pack, Phys. Rev. B 13 (1976) 5188.
[27] P. Pulay, Chem. Phys. Lett. 73 (1980) 393.
[28] When the initial configuration of astoms in the cell was symmetric, the final configuration was also symmetric. The two excess electrons were distributed among the four nearest-neighbor Ce atoms around the oxygen vacancy site, where these Ce ions each gain about 0.5 electrons.
[29] When we assumed an antiferromagnetic spin configuration between Ce(1) and Ce(2), we obtained a solution that was energetically degenerated with the ferromagnetic solution.